Onset of Spinal Cord Astrocyte Precursor Emigration from the Ventricular Zone Involves the Zeb1 Transcription Factor

David Ohayon, Alain Garcès, Willy Joly, Chadi Soukkarieh, Tsuyoshi Takagi, Jean-Charles Sabourin, Eric Agius, Douglas Darling, Pascal de Santa Barbara, Yujiro Higashi, et al.

Onset of Spinal Cord Astrocyte Precursor Emigration from the Ventricular Zone Involves the Zeb1 Transcription Factor

David Ohayon,[1,4,8,9] Alain Garcès,[1,9] Willy Joly,[1] Chadi Soukkarieh,[1,2] Tsuyoshi Takagi,[3] Jean-Charles Sabourin,[1] Eric Agius,[4] Douglas S. Darling,[5] Pascal De Santa Barbara,[6] Yujiro Higashi,[3] Claus C. Stolt,[7] Jean-Philippe Hugnot,[1] William D. Richardson,[8] Patrick Carroll,[1] and Alexandre Pattyn[1,10,*]

[1]INSERM U1051, Institut des Neurosciences de Montpellier, 34091 Montpellier, France
[2]Department of Animal Biology, Faculty of Sciences, Damascus University, Damascus, Syria
[3]Department of Perinatology, Institute for Developmental Research, Aichi Human Service Center, Kasugai, Aichi 480-0392, Japan
[4]Université de Toulouse, Centre National de la Recherche Scientifique (CNRS), CBD-UMR5547, 31062 Toulouse, France
[5]Department of Oral Immunology and Infectious Diseases, University of Louisville, Louisville, KY 40202, USA
[6]PhyMedExp, INSERM U1046, CNRS UMR 9214, University of Montpellier, 34295 Montpellier, France
[7]Institut für Biochemie, Emil-Fischer-Zentrum, Universität Erlangen-Nürnberg, 91054 Erlangen, Germany
[8]Wolfson Institute for Biomedical Research, University College London, London WC1E 6BT, UK
[9]Co-first author
[10]Lead Contact
*Correspondence: alexandre.pattyn@inserm.fr

SUMMARY

During spinal cord development, astrocyte precursors arise from neuroepithelial progenitors, delaminate from the ventricular zone, and migrate toward their final locations where they differentiate. Although the mechanisms underlying their early specification and late differentiation are being deciphered, less is known about the temporal control of their migration. Here, we show that the epithelial-mesenchymal transition regulator Zeb1 is expressed in glial precursors and report that loss of *Zeb1* function specifically delays the onset of astrocyte precursor delamination from the ventricular zone, correlating with transient deregulation of the adhesion protein Cadherin-1. Consequently, astrocyte precursor invasion into the *Zeb1*$^{-/-}$ mutant white matter is delayed, and induction of their differentiation is postponed. These findings illustrate how fine regulation of adhesive properties influences the onset of neural precursor migration and further support the notion that duration of exposure of migrating astrocyte precursors to environmental cues and/or their correct positioning influence the timing of their differentiation.

INTRODUCTION

Oligodendrocytes and astrocytes constitute the main glial cell populations of neural origin within the CNS. During embryogenesis, glial precursors arise from neural stem cells located in the ventricular zone (VZ), after a primary phase of neurogenesis, delaminate and migrate toward their final locations where they differentiate. In the developing spinal cord, oligodendrocyte precursors (OPs) are generated from specific progenitor domains along the dorsoventral (DV) axis, while astrocyte precursors (APs) are produced from all progenitor domains in a ventral-to-dorsal temporal sequence (Rowitch and Kriegstein, 2010; Tripathi et al., 2011; Tien et al., 2012). The molecular mechanisms controlling the gliogenic switch are beginning to be deciphered and involve the Sox9 transcription factor that acts upstream of NFIa to coordinate the arrest of neurogenesis and initiation of gliogenesis (Stolt et al., 2003; Deneen et al., 2006; Kang et al., 2012). Also, extensive studies have identified several key signaling pathways and transcriptional regulators controlling OP and AP differentiation (Kessaris et al., 2008; Rowitch and Kriegstein, 2010; Emery and Lu, 2015).

In contrast, relatively less is known about the time window during which newly specified OPs and APs have to exit the VZ and invade the mantle zone (MZ). Zeb1 and Zeb2 form a small family of transcription factors involved in many developmental and physiopathological processes, including epithelial-mesenchymal transitions (EMTs) and the formation of neural crest-derived tissues (Van de Putte et al., 2003; Gheldof et al., 2012; Rogers et al., 2013; Ohayon et al., 2015). Recent findings have established that *Zeb2* controls OP maturation around birth (Weng et al., 2012). Here we show that Zeb1 is expressed in embryonic glial precursors and report its implication in the temporal control of AP migration.

RESULTS AND DISCUSSION

Zeb1 and Zeb2 Exhibit Dynamic Expression Profiles in the Mouse Developing Spinal Cord

During the neurogenic phase of the developing spinal cord, between embryonic days (E)9.5 and 12.5, we observed increasing

levels of Zeb1 in VZ progenitors (Figures 1A, 1B, and 1J) that also expressed Zeb2 at these stages (Figures S1A–S1C and 1J). In the MZ, whereas Zeb2 was maintained in discrete neuronal populations (Figures S1C–S1E and 1J), Zeb1 was gradually downregulated in post-mitotic neurons, except in motoneurons (MNs; Figures 1B, 1C, 1F, and 1J). During the gliogenic phase, Zeb1 was maintained in VZ progenitors (Figures 1C–1E and 1J), while Zeb2 was downregulated from E12.5 and became undetectable in these cells by E13.5 (Figures S1C, S1D, and 1J). At E13.5, Zeb1-positive (+) cells were observed in the ventral MZ (Figures 1C and S1J), and their number increased subsequently with a spatial distribution reminiscent of glial precursors (Figures 1D, 1E, and S1K). At E18.5, we confirmed that Zeb1 was largely excluded from NeuN+ neuronal populations except in MNs (Figure 1F), but it was detected in Olig2+ OPs (Figures 1E, 1G, and 1J) and GFAP+ APs (Figures 1E, 1H, 1I, and 1J). In contrast, Zeb2 was excluded from migrating OPs and APs at early stages, but it was selectively induced in OPs from E16.5 (Figures S1F, S1G, and 1J; Weng et al., 2012).

At adulthood, Zeb1 was maintained in a small fraction of Sox10+ and Olig2+ cells (Figures 1K and 1L) that were negative for the mature oligodendrocyte marker CC1 (Figure 1M), indicating that they were adult OPs. Moreover, co-expression of Zeb1 with AldoC and GFAP (Figures 1N and 1O) showed that mature astrocytes maintained Zeb1. A similar pattern of Zeb1 was observed in the adult cortex (Figures S1L and S1M). Altogether, these data show the following: (1) during neurogenesis, spinal cord VZ progenitors express both Zeb2 and Zeb1, albeit at low levels, while only Zeb1 is robustly expressed in these cells during gliogenesis; (2) Zeb1 is maintained in migrating OPs and APs throughout embryogenesis; and (3) Zeb1 constitutes a specific marker for adult OPs and mature astrocytes.

Spinal Cord APs Are Selectively Affected in *Zeb1*$^{-/-}$ Mutants

These observations prompted us to assess glial cell formation in *Zeb1*$^{-/-}$ animals (Takagi et al., 1998; see Figures S1N–S1Q) by mainly focusing on the spinal cord. First, analysis of the spatiotemporal expression profile of OP determinants, including Olig2, *Sox10*, *PDGFr*α, and *PLP1* between E12.5 and E18.5, showed that Zeb1 is dispensable for the earliest phases of OP formation (Figures S2A–S2Q). In contrast, time course analysis of *Fgfr3* expression (Pringle et al., 2003) revealed a specific requirement for Zeb1 in APs. Indeed, in wild-type (WT) embryos, migrating *Fgfr3*+ APs in the MZ normally emerged in a ventral-to-dorsal sequence starting at E13.5, and they expanded to populate the entire width of the spinal cord by E18.5 (Figures 2A, 2C, 2E, 2G, 2I, and 2K; Tien et al., 2012). Strikingly, at E13.5, virtually no *Fgfr3*+ AP was detected in the MZ of *Zeb1*$^{-/-}$ embryos (Figure 2B). At E14.5, a few migrating APs were visualized, though at locations and in numbers reminiscent of WT at E13.5 (Figures 2A, 2D, 2M, and 2N). Also at E15.5, E16.5, and E17.5, the pattern of *Fgfr3*+ cells in the mutant MZ resembled that of WT at E14.5, E15.5, and E16.5, respectively (Figures 2C–2J).

Consistent with that, quantification revealed a deficit of APs in the MZ of *Zeb1*$^{-/-}$ embryos until E17.5 (Figures 2M and 2N). However, from E14.5, numbers of APs in the mutant MZ progressively increased similarly to WT, albeit with a 24-hr delay, and eventually they reached a close to normal complement by E18.5 (Figures 2K–2N). BrdU incorporation experiments performed at E16.5 revealed that the proportion of migrating *Fgfr3*+ APs that were also BrdU+ was comparable in both genotypes (11.31% ± 2.38% in WT versus 10.38% ± 2.42% in *Zeb1*$^{-/-}$ mutants; Figures 2O and 2P), showing that mutant APs proliferate normally on their migratory route. This suggested that the delayed apparition and transient deficit of APs in the MZ of *Zeb1*$^{-/-}$ mutants rather reflected a role for Zeb1 at early steps of their development.

To characterize this defect, we first assessed cell proliferation in the VZ at E13.5 by determining the proportion of Ki67+ cycling progenitors that have incorporated BrdU during a 2-hr pulse. In WT, divergences were observed along the DV axis (21.9% ± 2.45% dorsally versus 40.5% ± 4.9% ventrally), and no significant differences were found in the mutants (22.6% ± 2.56% dorsally versus 41.8% ± 4.6% ventrally; Figures 2Q and 2R), indicating that, at this stage, VZ progenitors proliferate at a normal rate in the absence of Zeb1. Next, extensive co-expression of Zeb1 with Sox9 (Figures S1H–S1K) and apparent phenotypic similarities between *Zeb1*$^{-/-}$ and *Sox9*$^{\Delta/\Delta}$ mutants in which the gliogenic switch is delayed by 24 hr (Stolt et al., 2003) prompted us to test whether Zeb1 could influence similar processes. First, analysis of Sox9 and NFIa expression in VZ progenitors of *Zeb1*$^{-/-}$ embryos revealed no difference compared to WT (Figures 2S–2X), though, at E13.5, there were reduced numbers of Sox9+ cells in the mutant MZ and virtually all the remaining ones were Olig2+ OPs (Figures 2W and 2X). This further illustrated that, while migrating OPs were detected on time in the mutants, APs were specifically affected. Second, we established that loss of *Sox9* function did not affect Zeb1 expression, thus revealing no epistatic relationships between the two factors (Figures S1R and S1S). Third, we analyzed *Aldh1l1*, whose onset of expression in the VZ is a good landmark of AP specification. Indeed, *Aldh1l1* was induced at E12.5 in the ventralmost domain of the VZ from which the first migrating APs arise 1 day later, and it expanded dorsally at E13.5 (Figures 2Y and 2AA; Tien et al., 2012). Analysis of *Zeb1*$^{-/-}$ mutants revealed that, although at E13.5 virtually no *Aldh1l1*+ AP was detected in the MZ, the spatiotemporal profile of *Aldh1l1* in the VZ appeared normal (Figures 2Z and 2AB), supporting the view that loss of Zeb1 function does not perturb the timing of AP specification. In line with this, analysis of spinal cord neuronal populations did not reveal any significant changes in *Zeb1*$^{-/-}$ animals (Figures S3A and S3B), in contrast to *Sox9*$^{\Delta/\Delta}$ embryos (Stolt et al., 2003), indicating that Zeb1 is dispensable for the gliogenic switch. We also excluded a role for Zeb1 in early survival of APs (Figure S3C). We finally determined that loss of *Zeb1* function did not affect the expression of patterning genes, including *Nkx2-2*, *Nkx6-1*, or *Pax6* (Figure S3D). Consistent with that, positional identity of APs that exhibit complementary expression of *Slit1* and *Reelin* according to their origin along the DV axis (Hochstim et al., 2008) was preserved in the mutants, albeit with a 24-hr delay (Figure S3E).

Altogether, these data show that AP specification, proliferation, survival, and positional identity appear normal in *Zeb1*$^{-/-}$ embryos, suggesting that delayed AP invasion into the mutant MZ rather reflected impaired migration.

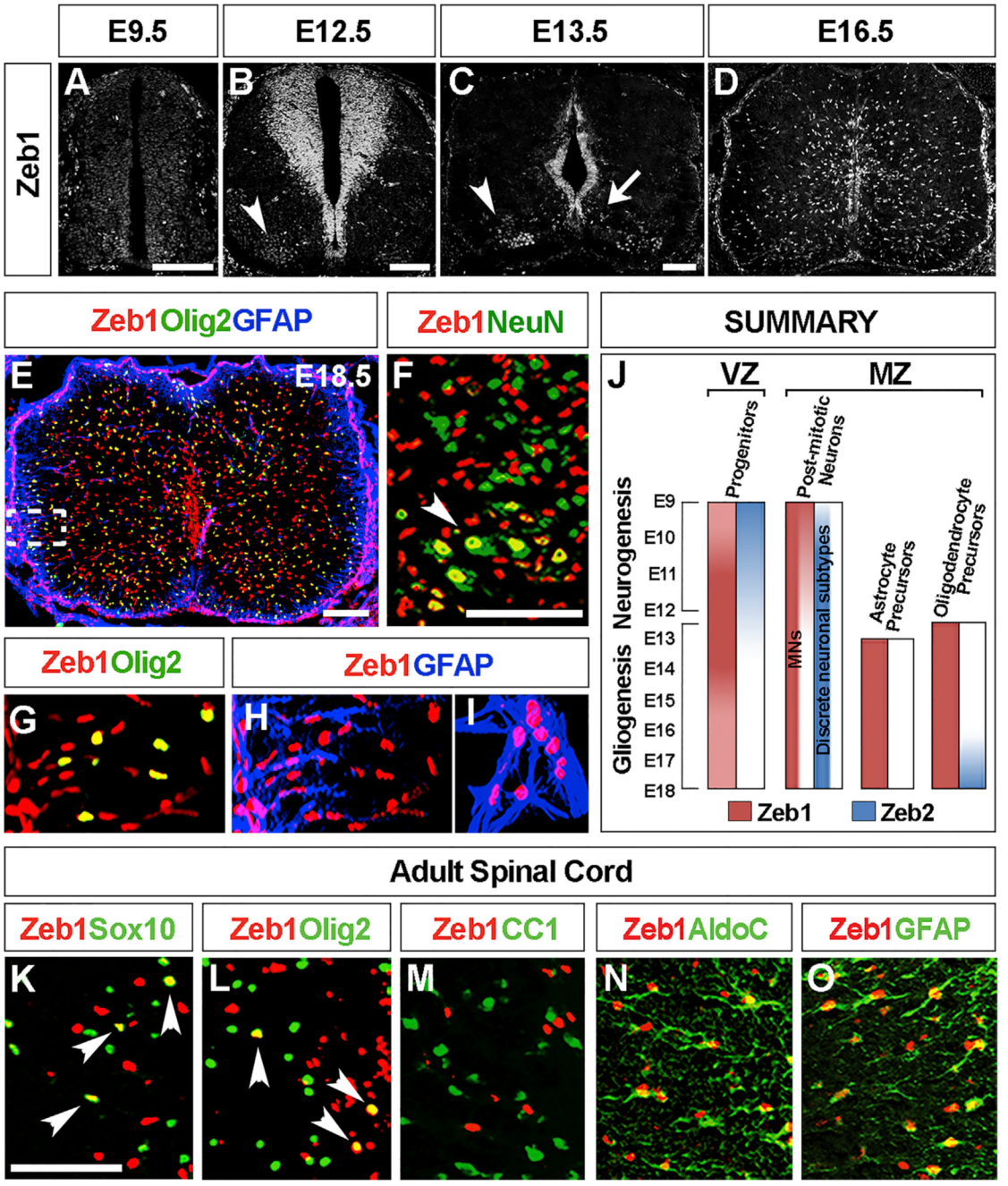

Figure 1. Zeb1 Expression in the Embryonic and Adult Spinal Cords

(A–D) Immunofluorescent staining for Zeb1 on thoracic spinal cord transverse sections of WT embryos at the indicated stages. Arrowheads in (B) and (C) point to Zeb1+ MNs. Arrows in (C) point to Zeb1+ cells in the ventral MZ.

(E) Triple immunostaining for Zeb1 (red), Olig2 (green), and GFAP (blue) on E18.5 thoracic spinal cord transverse sections. The white dotted frame indicates the position of close ups shown in (G) and (H).

(F) High-magnification image of E18.5 thoracic spinal cord transverse sections stained with Zeb1 and NeuN. Arrowhead points to Zeb1+/NeuN+ MNs.

(G and H) High-magnification images show E18.5 thoracic spinal cord transverse sections stained with Zeb1 and either Olig2 (G) or GFAP (H).

(I) Cultured astrocytes prepared at E18.5 were stained with Zeb1 and GFAP.

(J) Summary shows the dynamic expression profiles of Zeb1 and Zeb2 in the embryonic spinal cord during the neurogenic and gliogenic phases.

(K–O) Ventrolateral views show adult thoracic spinal cord transverse sections stained with Zeb1 and Sox10 (K), Olig2 (L), CC1 (M), AldoC (N), or GFAP (O).

Scale bars, 100 μm. See also Figure S1.

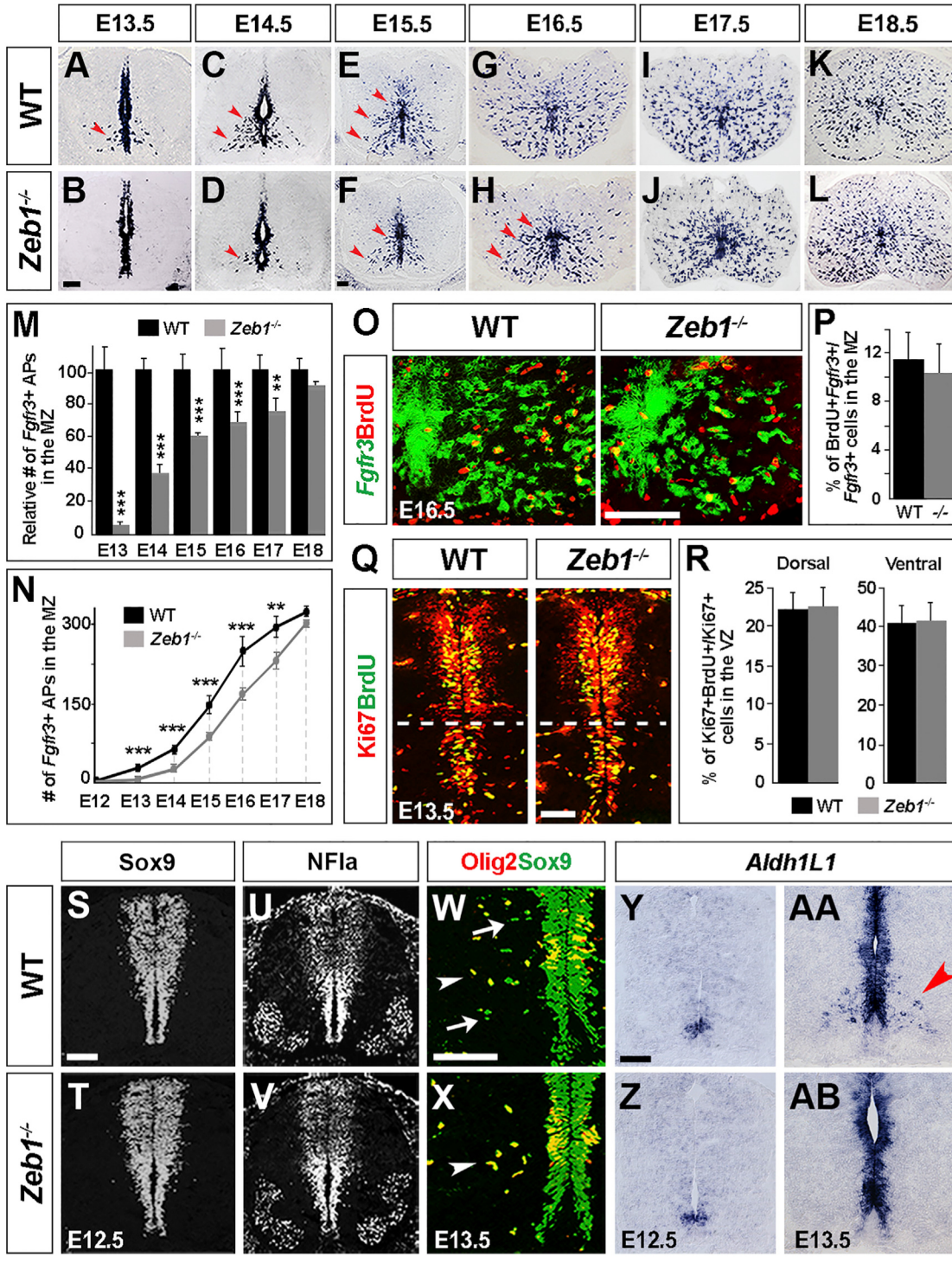

Figure 2. Delayed Apparition of APs in the MZ of *Zeb1*$^{-/-}$ Embryos

(A–L) In situ hybridization for *Fgfr3* on thoracic spinal cord transverse sections from WT and *Zeb1*$^{-/-}$ embryos between E13.5 and E18.5. Arrowheads point to migrating streams of APs.

(M) Relative quantification of migrating APs in the MZ of WT and *Zeb1*$^{-/-}$ embryos between E12.5 and E18.5 is shown.

(N) Numbers of migrating APs in the MZ of WT and *Zeb1*$^{-/-}$ embryos from E12.5 to E18.5 are shown.

(O) Combined in situ hybridization for *Fgfr3* (transformed in green pseudo-color) and immunostaining for BrdU (red) on thoracic spinal cord transverse sections at E16.5 from WT and *Zeb1*$^{-/-}$ mutants after a 2-hr pulse are shown.

(P) Quantification of the proportion of *Fgfr3*+ migrating APs that have incorporated BrdU after a 2-hr pulse at E16.5 in WT and *Zeb1*$^{-/-}$ (−/−) embryos is shown.

(legend continued on next page)

Onset of AP Emigration from the Spinal Cord VZ Is Delayed in *Zeb1*$^{-/-}$ Embryos

To assess AP migration, we took advantage of the singular expression profile of the extracellular matrix glycoprotein TnC (Karus et al., 2011). Indeed, in WT embryos, TnC was not detected in the VZ at E12.5 (Figure S4A), but it was homogenously induced at E13.5 except in the most ventral VZ domain, which only exhibited scattered expression (Figures 3A and S4B). Nevertheless, APs migrated out of this domain and *TnC*+ APs were detected in the MZ adjacent to it (Figures 3A, S4B, and S4C), showing that at ventral positions *TnC* is mainly induced once APs have initiated their migration. In *Zeb1*$^{-/-}$ embryos, *TnC* was normally induced at E13.5, but, whereas no *TnC*+ AP was found in the MZ at this stage, many *TnC*+ cells were concomitantly observed in the ventral VZ domain abutting the floor plate (Figure 3B), a phenotype still evident at E14.5 and E15.5 (Figures 3C–3G). In addition, at E16.5, but not E17.5, clusters of *TnC*+ cells were still abnormally detected in the dorsal VZ domain of *Zeb1*$^{-/-}$ embryos (Figures 3H–3K). These data show that, in *Zeb1*$^{-/-}$ mutants, newly specified APs remain transiently blocked in the VZ and start to migrate with a 24-hr delay.

Relatively little is known about the molecular determinants controlling the onset of AP migration, although roles for *TnC* itself (Karus et al., 2011) and *Apcdd1* (Kang et al., 2012) have been proposed. However, analyses of both markers in *Zeb1*$^{-/-}$ embryos did not reveal any alteration of their expression (Figures 3A, 3B, S4D, and S4E), suggesting alternative mechanisms. Zeb1 is a major regulator of EMT, notably acting through direct repression of the gene encoding the adhesion molecule Cadherin-1 (Cdh1; Gheldof et al., 2012). Chromatin immunoprecipitation (ChIP) assays performed on E13.5 spinal cords revealed that Zeb1 actually binds proximal regions of the *Cdh1* promoter in vivo (Figure 3L), prompting us to assess its expression in the mutants. In contrast to WT spinal cords in which Cdh1 expression was under detectable thresholds at all stages analyzed, in *Zeb1*$^{-/-}$ embryos Cdh1 was ectopically detected in the VZ, first ventrally at E12.5, then in more dorsal regions until E16.5 (Figure 3M). This result is strikingly reminiscent of the deregulation of Cdh1 previously described in several brain regions of *Zeb1*$^{-/-}$ mutants at late embryonic stages (Liu et al., 2008). In many tissues and cancer cells, the presence of Cdh1 is incompatible with a migratory phenotype (Gheldof and Berx, 2013). In line with this, ex ovo electroporation of E6 chick spinal cords that were cultured as explants for 48 hr showed that Cdh1-transfected cells had a significantly higher tendency to remain in the VZ compared to cells transfected with a control vector (Figures 3N–3P). Thus, transient derepression of Cdh1 may provide one mechanism by which the onset of AP emigration is impaired in *Zeb1*$^{-/-}$ mutants. It is of note that levels of ectopic Cdh1 were lower compared to its endogenous expression sites (insets in Figure 3M) and that no Cdh1+ cells were observed in the MZ when mutant APs eventually delaminated (Figure 3M), suggesting that other determinants act in parallel to Zeb1 to finally repress *Cdh1*.

Interestingly, these findings illustrate some similarities between the processes of AP delamination from the VZ and EMT, and they are highly reminiscent of the impaired migration of neural crest cells consequent to *Zeb2* knockdown, reflecting deregulation of *Cdh1* in the dorsal neural tube at early stages (Van de Putte et al., 2003; Rogers et al., 2013). They are also strikingly evocative of the function of Scratch1/2 transcription factors in controlling the onset of cortical neuron precursor migration through repression of *Cdh1* (Itoh et al., 2013). To a lesser extent, they recall the role of Foxp2/4 proteins in repressing Cdh2 in young spinal cord neurons, thus allowing their detachment from the VZ (Rousso et al., 2012), though we did not observe obvious alteration of Cdh2 expression in *Zeb1*$^{-/-}$ mutants (Figures S4F and S4G). Altogether, these data show that fine regulation of cell-adhesive properties appears as a widespread process involving multiple families of transcriptional regulators at distinct stages and locations throughout the developing nervous system, which influences neural precursor migration.

Intriguingly, in contrast to APs, OP migration occurred on time in *Zeb1*$^{-/-}$ mutants. This may reflect that OPs start to migrate earlier than APs, at around E12.5 (Figures S2R and S2S; Touahri et al., 2012). At that time, there was no deregulation of Cdh1 in the mutant Olig2+ domain (Figures S2T and S2U), and Zeb2 expression was still ongoing in the VZ, albeit at low levels (Figure S1C). In the same line, no obvious defect was observed during the earlier neurogenic phase in *Zeb1*$^{-/-}$ embryos. During this period, Zeb2 was expressed in the VZ and Zeb1 was only detected at low levels (Figures 1A and S1A–S1C). Thus, although roles for Zeb1 during neurogenesis and oligodendrogenesis cannot be totally ruled out, the dynamic spatiotemporal profile and levels of Zeb proteins combined with possible functional redundancies may account for the apparent specific requirement of Zeb1 in APs.

Early Defects of AP Migration or Specification Later Perturb Their Differentiation

At spinal levels, induction of the GFAP protein is a classic indicator of the differentiation of AP subtypes, starting at around E16.5 when cells have reached the pial surface of the spinal cord (Rowitch and Kriegstein, 2010; Hong and Song, 2014). At this stage, analysis of *Zeb1*$^{-/-}$ embryos revealed that fewer APs had settled

(Q) Double-immunofluorescent staining for Ki67 and BrdU on thoracic spinal cord transverse sections at E13.5 from WT (left panel) and *Zeb1*$^{-/-}$ (right panel) embryos after a 2-hr pulse of BrdU is shown.

(R) Quantification of the proportion of Ki67+/BrdU+ cells over the Ki67+ population in dorsal (left graph) and ventral (right graph) regions of the VZ after a 2-hr pulse of BrdU at E13.5 in WT and *Zeb1*$^{-/-}$ embryos is shown.

(S–V) Immunofluorescent staining for Sox9 (S and T) and NFIa (U and V) on thoracic spinal cord transverse sections from WT and *Zeb1*$^{-/-}$ embryos at E12.5 is shown.

(W and X) Ventrolateral views of thoracic spinal cord transverse sections from WT and *Zeb1*$^{-/-}$ embryos at E13.5 stained with Sox9 and Olig2 antibodies. Arrowheads point to Sox9+/Olig2+ OPs that are present in both genotypes, while arrows point to Sox9+/Olig2− APs that are only detected in WT.

(Y–AB) In situ hybridization for *Aldh1L1* on thoracic spinal cord transverse sections from WT and *Zeb1*$^{-/-}$ mutants at E12.5 (Y and Z) and E13.5 (AA and AB). Arrowhead in (AA) points toward migrating APs in the ventral MZ.

Scale bars, 100 μm. In (M), (N), (P), and (R), data are represented as mean ± SEM (**p < 0.01 and ***p < 0.001). See also Figures S1–S3.

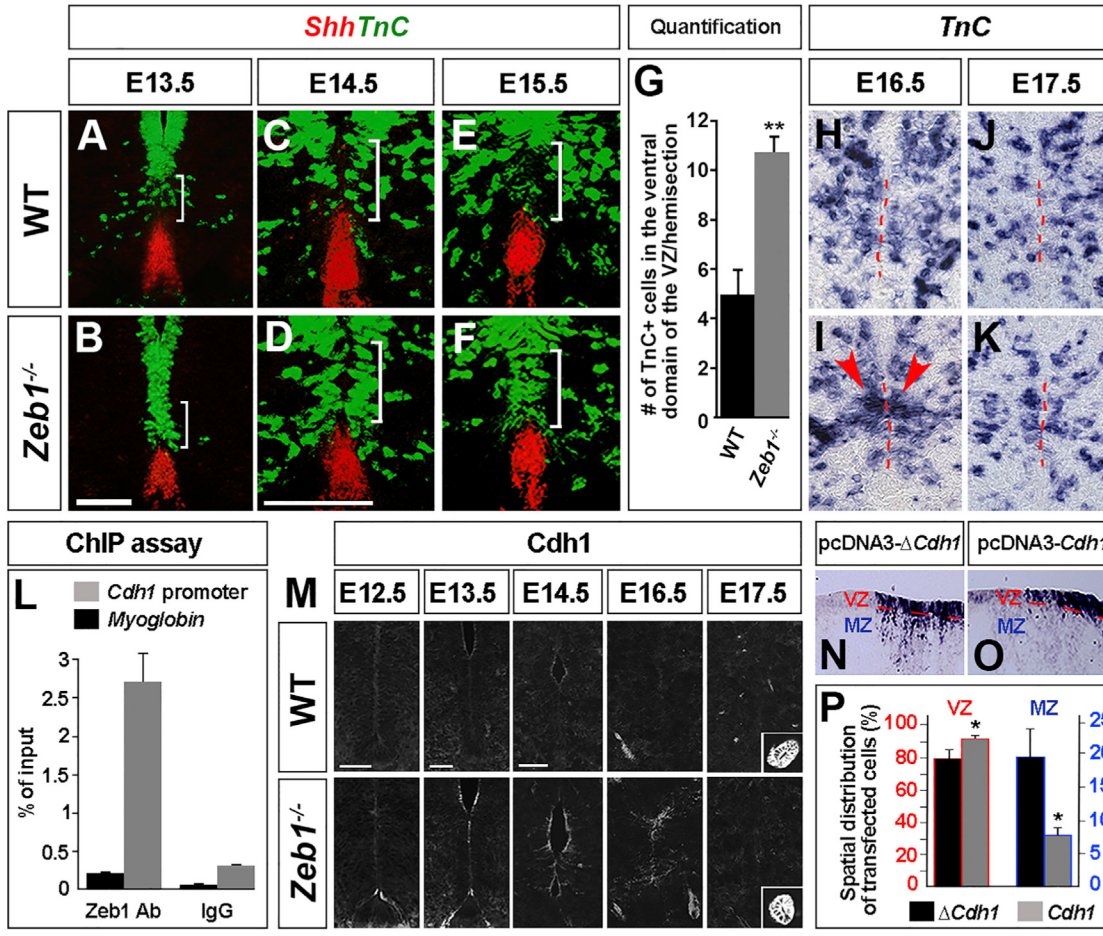

Figure 3. Zeb1 Controls the Onset of AP Emigration from the VZ

(A–F) Double in situ hybridization for *Shh* (red) and *TnC* (transformed in green pseudo-color) on thoracic spinal cord transverse sections of WT and *Zeb1*$^{-/-}$ mutants at E13.5 (A and B), E14.5 (C and D), and E15.5 (E and F). Brackets delineate the ventral VZ domain abutting the *Shh*+ floor plate.

(G) Quantification of *TnC*+ cells in the ventral VZ domain of WT and *Zeb1*$^{-/-}$ embryos at E14.5 is shown.

(H–K) In situ hybridization for *TnC* on thoracic spinal cord transverse sections from WT and *Zeb1*$^{-/-}$ embryos at E16.5 (H and I) and E17.5 (J and K). Arrowheads in (I) point to dorsal groups of *TnC*+ in the dorsal VZ of the mutants at E16.5. Red dotted lines delineate the central canal.

(L) qPCR from ChIP assays performed on E13.5 spinal cords with a Zeb1 antibody (Ab) or control IgG, using primers flanking Zeb1-binding sites in the *Cdh1* promoter, or located in the *Myoglobin* gene as a negative control. Data are represented as percentage of input DNA.

(M) Representative images of the VZ of WT and *Zeb1*$^{-/-}$ embryos stained for Cdh1 at the indicated stages. Note that levels of ectopic Cdh1 expression in the mutant are lower than in its endogenous sites, as shown in kidney tubules (insets in right panels).

(N and O) Transverse sections of chick spinal cord explants cultured for 48 hr after electroporation at E6 of expression vectors either containing a truncated form of the *Cdh1* cDNA (N, *pcDNA3-ΔCdh1*) or the full-length *Cdh1* cDNA (O, *pcDNA3-Cdh1*), stained by in situ hybridization with a probe recognizing both mRNAs. Red dotted lines delimit the VZ and MZ.

(P) Spatial distribution of cells expressing either Δ*Cdh1* or *Cdh1* in the VZ (left graph) and in the MZ (right graph) is shown.

Data are represented as mean ± SEM (**p < 0.01 and *p < 0.005). Scale bars, 100 μm. See also Figures S2 and S4.

at the margin of the spinal cord compared to WT (Figures 4A and 4B), consistent with the fact that they leave the VZ in a delayed manner. Strikingly, in parallel we found that GFAP expression was reduced in the mutant white matter compared to WT and was not concomitantly ectopically detected in the gray matter (Figures 4D and 4E). This suggested that early delay of AP migration later perturbs the timing of their differentiation.

To further test this issue, we analyzed *Sox9*$^{\Delta/\Delta}$ mutants in which glial cell specification and, in turn, migration were delayed by 24 hr. In agreement with previous findings (Stolt et al., 2003), we observed that at E16.5 fewer APs had invaded the mutant white matter (Figure 4C), and we found that GFAP expression also was reduced at this stage (Figure 4F), thus echoing the *Zeb1*$^{-/-}$ mutant phenotype. By E18.5, however, robust expression of GFAP was observed ventrally in *Zeb1*$^{-/-}$ embryos (arrowheads in Figures 4G and 4H), which correlated with the presence of numerous *Fgfr3*+/*Slit1*+ APs in the ventral white matter (arrowheads in Figures 4I–4L). At more dorsal positions, however, levels of GFAP were still slightly reduced compared to WT (brackets in Figures 4G and 4H), correlating with fewer *Fgfr3*+/*Reelin*+ cells located at the margin of the mutant spinal cord compared to WT (brackets in Figures 4I, 4J, 4M, and 4N). These

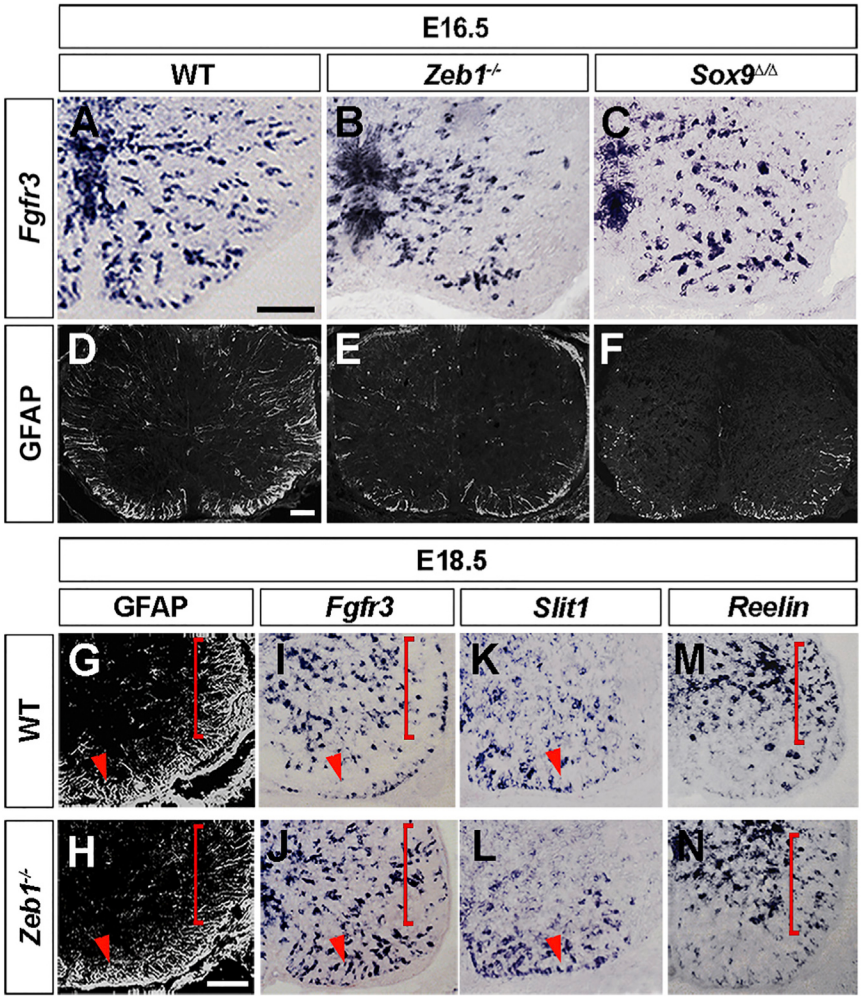

Figure 4. Delayed Induction of GFAP in *Zeb1*$^{-/-}$ and *Sox9*$^{\Delta/\Delta}$ Mutants Correlates with Mis-positioning of APs in the White Matter

(A–C) Ventrolateral views show E16.5 thoracic spinal cord transverse sections from WT, *Zeb1*$^{-/-}$, and *Sox9*$^{\Delta/\Delta}$ embryos stained by in situ hybridization with an *Fgfr3* probe.

(D–F) Immunofluorescent staining for GFAP on thoracic spinal cord transverse sections from WT, *Zeb1*$^{-/-}$, and *Sox9*$^{\Delta/\Delta}$ embryos is shown.

(G–N) Ventrolateral views of E18.5 thoracic spinal cord transverse sections from WT and *Zeb1*$^{-/-}$ embryos, showing GFAP (G and H), *Fgfr3* (I and J), *Slit1* (K and L), and *Reelin* (M and N) expression. Arrowheads point to the ventral white matter exhibiting a high level of GFAP expression in both genotypes, which correlates with the presence of numerous *Fgfr3*+ and *Slit1*+ APs. Brackets point to reduced GFAP expression at more dorsal positions in the mutants compared to WT, correlating with reduced numbers of *Fgfr3*+ and *Reelin*+ APs at the margin of the mutant spinal cord. Scale bars, 100 μm.

results thus show that early defects of AP migration or specification, respectively, in *Zeb1*$^{-/-}$ and *Sox9*$^{\Delta/\Delta}$ mutants are later associated with delayed invasion of the white matter by APs and postponed induction of GFAP. These data further support the notion that duration of AP exposure to environmental cues and/or their correct positioning influence the timing of their differentiation (Barnabé-Heider et al., 2005; Hong and Song, 2014).

It is of note that the embryonic lethality of *Zeb1*-deficient mice precluded full assessment of glial cell differentiation that largely proceeds at post-natal stages. Moreover, the fact that at adulthood Zeb1 is specifically maintained in mature astrocytes and adult OPs, which both retain some precursor-like properties and migratory capacities, leaves open the possibility that this transcriptional regulator also may influence adult gliogenesis. Conditional knockdown approaches will certainly help to address these issues.

EXPERIMENTAL PROCEDURES

Mouse Strains

Procedures involving animals and their care were conducted according to the French Ministry of Agriculture and the European Community Council Directive no. 86/609/EEC, OJL 358. Protocols were validated by the Direction Départementale des Services Vétérinaires de l'Hérault (Certificate of Animal Experimentation no. 34-376). *Zeb1*$^{-/-}$ and *Sox9*$^{\Delta/\Delta}$ embryos were obtained and genotyped as previously described (Takagi et al., 1998; Stolt et al., 2003).

Astrocyte Culture

Astrocytes were prepared from E18 WT embryos as previously described (Perraud et al., 1990).

Histological Analyses

Simple or double in situ hybridization and immunofluorescent staining on cryosections were performed as previously described (Ventéo et al., 2012). Antisense RNA probes for *Aldh1L1*, *Apcdd1*, *Chx10*, *Fgfr3*, *Gata3*, *Lbx1*, *Nkx2-2*, *Nkx6-1*, *Pax6*, *PdgfRα*, *PLP1*, *Reelin*, *Sim1*, *Slit1*, *Shh*, *Sox10*, *Tlx3*, and *TnC* were used. Antibodies used in this study were as follows: goat AldoC (Santa Cruz Biotechnology), mouse APC (clone CC1; Calbiochem), rat BrdU (Abcam), rat Cadherin-1 (Alexis Biochemicals), rabbit Cadherin-2 (Abcam), rabbit and mouse GFAP (Dako), rabbit Ki67 (Abcam), mouse NeuN (Millipore), rabbit NFIa (Active Motif), goat Olig2 (Santa Cruz Biotechnology), goat Sox2 (Abcam), rabbit Sox9 (Stolt et al., 2003), guinea pig Sox10 (gift of M. Wegner), rabbit Zeb1 (Darling et al., 2003), and rabbit Zeb2 (Santa Cruz Biotechnology). Alexa Fluor 594-, 488-, or 647-conjugated secondary antibodies (Thermo Fisher Scientific) were used. Apoptosis was assessed using the ApopTag peroxidase detection kit (Millipore). For proliferation assays, BrdU (Sigma) was injected intraperitoneally into pregnant mice (2 mg/animal) at E13.5 or E16.5, 2 hr before sacrifice. For BrdU detection, slides were incubated in 10 mM sodium citrate buffer (pH 6.0) at 95°C for 15 min, then at room temperature (RT) for 15 min, and subjected to immunostaining. For double *Fgfr3*/BrdU experiments, *Fgfr3* in situ hybridization was performed first.

ChIP

ChIP assay was performed as previously described (Nègre et al., 2006) on 30 E13.5 WT spinal cords dissected clear of surrounding tissues. Rabbit-polyclonal antiserum for ZEB1 (H-102, Santa Cruz Biotechnology) and control rabbit IgG (sc-2027, Santa Cruz Biotechnology) were used. Promoter occupancy was assessed by quantitative real-time PCR using primers in the *Cadherin-1*

promoter (forward: 5′-AGACAGGGGTGGAGGAAGTT-3′; reverse: 5′-GGGC AGGAGTCTAGCAGAAG-3′) or the *Myoglobin* gene as control. For each condition, two biological and two technical replicates were performed.

Chick Electroporation

This was performed as previously described (Touahri et al., 2012) using a pcDNA3-Cdh1 expression vector (gift of P. Cossart) or a truncated form of the same vector (pcDNA3-ΔCdh1).

Cell Counts

Quantification in mice was carried out on three independent embryos of each genotype. For chick experiments, two independent experiments were performed and sections from four explants for each condition were analyzed. Cell counts were performed using the ImageJ software.

Statistical Analyses

Quantitative analyses were statistically analyzed using Student's t test and represented as mean ± SEM.

AUTHOR CONTRIBUTIONS

Conceptualization, D.O., A.G., W.J., E.A., and A.P.; Investigation, D.O., A.G., W.J., C.S., and A.P.; Resources, T.T., J.-C.S., J.-P.H., Y.H., C.C.S., D.S.D., P.D.S.B., and W.D.R.; Supervision, E.A., W.D.R., P.C., and A.P.; Writing – Original Draft, A.P.; Writing – Review & Editing, P.C. and A.P.

ACKNOWLEDGMENTS

We thank S. Faure and S. Valleix for technical help and discussions. We are grateful to B. Schuttengruber for sharing his expertise on ChIP assays. We also thank E. Andersson, J. Briscoe, P. Cossart, J. Ericson, A. Faissner, E. Gouin, M. Karus, J. Nardelli, and M. Wegner for the kind gifts of materials. This work was funded by Inserm and CNRS.

REFERENCES

Barnabé-Heider, F., Wasylnka, J.A., Fernandes, K.J., Porsche, C., Sendtner, M., Kaplan, D.R., and Miller, F.D. (2005). Evidence that embryonic neurons regulate the onset of cortical gliogenesis via cardiotrophin-1. Neuron *48*, 253–265.

Darling, D.S., Stearman, R.P., Qi, Y., Qiu, M.S., and Feller, J.P. (2003). Expression of Zfhep/deltaEF1 protein in palate, neural progenitors, and differentiated neurons. Gene Expr. Patterns *3*, 709–717.

Deneen, B., Ho, R., Lukaszewicz, A., Hochstim, C.J., Gronostajski, R.M., and Anderson, D.J. (2006). The transcription factor NFIA controls the onset of gliogenesis in the developing spinal cord. Neuron *52*, 953–968.

Emery, B., and Lu, Q.R. (2015). Transcriptional and epigenetic regulation of oligodendrocyte development and myelination in the central nervous system. Cold Spring Harb. Perspect. Biol. *7*, a020461.

Gheldof, A., and Berx, G. (2013). Cadherins and epithelial-to-mesenchymal transition. Prog. Mol. Biol. Transl. Sci. *116*, 317–336.

Gheldof, A., Hulpiau, P., van Roy, F., De Craene, B., and Berx, G. (2012). Evolutionary functional analysis and molecular regulation of the ZEB transcription factors. Cell. Mol. Life Sci. *69*, 2527–2541.

Hochstim, C., Deneen, B., Lukaszewicz, A., Zhou, Q., and Anderson, D.J. (2008). Identification of positionally distinct astrocyte subtypes whose identities are specified by a homeodomain code. Cell *133*, 510–522.

Hong, S., and Song, M.R. (2014). STAT3 but not STAT1 is required for astrocyte differentiation. PLoS ONE *9*, e86851.

Itoh, Y., Moriyama, Y., Hasegawa, T., Endo, T.A., Toyoda, T., and Gotoh, Y. (2013). Scratch regulates neuronal migration onset via an epithelial-mesenchymal transition-like mechanism. Nat. Neurosci. *16*, 416–425.

Kang, P., Lee, H.K., Glasgow, S.M., Finley, M., Donti, T., Gaber, Z.B., Graham, B.H., Foster, A.E., Novitch, B.G., Gronostajski, R.M., and Deneen, B. (2012). Sox9 and NFIA coordinate a transcriptional regulatory cascade during the initiation of gliogenesis. Neuron *74*, 79–94.

Karus, M., Denecke, B., ffrench-Constant, C., Wiese, S., and Faissner, A. (2011). The extracellular matrix molecule tenascin C modulates expression levels and territories of key patterning genes during spinal cord astrocyte specification. Development *138*, 5321–5331.

Kessaris, N., Pringle, N., and Richardson, W.D. (2008). Specification of CNS glia from neural stem cells in the embryonic neuroepithelium. Philos. Trans. R. Soc. Lond. B Biol. Sci. *363*, 71–85.

Liu, Y., El-Naggar, S., Darling, D.S., Higashi, Y., and Dean, D.C. (2008). Zeb1 links epithelial-mesenchymal transition and cellular senescence. Development *135*, 579–588.

Nègre, N., Lavrov, S., Hennetin, J., Bellis, M., and Cavalli, G. (2006). Mapping the distribution of chromatin proteins by ChIP on chip. Methods Enzymol. *410*, 316–341.

Ohayon, D., Ventéo, S., Sonrier, C., Lafon, P.A., Garcès, A., Valmier, J., Rivat, C., Topilko, P., Carroll, P., and Pattyn, A. (2015). Zeb family members and boundary cap cells underlie developmental plasticity of sensory nociceptive neurons. Dev. Cell *33*, 343–350.

Perraud, F., Labourdette, G., Eclancher, F., and Sensenbrenner, M. (1990). Primary cultures of astrocytes from different brain areas of newborn rats and effects of basic fibroblast growth factor. Dev. Neurosci. *12*, 11–21.

Pringle, N.P., Yu, W.P., Howell, M., Colvin, J.S., Ornitz, D.M., and Richardson, W.D. (2003). Fgfr3 expression by astrocytes and their precursors: evidence that astrocytes and oligodendrocytes originate in distinct neuroepithelial domains. Development *130*, 93–102.

Rogers, C.D., Saxena, A., and Bronner, M.E. (2013). Sip1 mediates an E-cadherin-to-N-cadherin switch during cranial neural crest EMT. J. Cell Biol. *203*, 835–847.

Rousso, D.L., Pearson, C.A., Gaber, Z.B., Miquelajauregui, A., Li, S., Portera-Cailliau, C., Morrisey, E.E., and Novitch, B.G. (2012). Foxp-mediated suppression of N-cadherin regulates neuroepithelial character and progenitor maintenance in the CNS. Neuron *74*, 314–330.

Rowitch, D.H., and Kriegstein, A.R. (2010). Developmental genetics of vertebrate glial-cell specification. Nature *468*, 214–222.

Stolt, C.C., Lommes, P., Sock, E., Chaboissier, M.C., Schedl, A., and Wegner, M. (2003). The Sox9 transcription factor determines glial fate choice in the developing spinal cord. Genes Dev. *17*, 1677–1689.

Takagi, T., Moribe, H., Kondoh, H., and Higashi, Y. (1998). DeltaEF1, a zinc finger and homeodomain transcription factor, is required for skeleton patterning in multiple lineages. Development *125*, 21–31.

Tien, A.C., Tsai, H.H., Molofsky, A.V., McMahon, M., Foo, L.C., Kaul, A., Dougherty, J.D., Heintz, N., Gutmann, D.H., Barres, B.A., and Rowitch, D.H. (2012). Regulated temporal-spatial astrocyte precursor cell proliferation involves BRAF signalling in mammalian spinal cord. Development *139*, 2477–2487.

Touahri, Y., Escalas, N., Benazeraf, B., Cochard, P., Danesin, C., and Soula, C. (2012). Sulfatase 1 promotes the motor neuron-to-oligodendrocyte fate switch by activating Shh signaling in Olig2 progenitors of the embryonic ventral spinal cord. J. Neurosci. *32*, 18018–18034.

Tripathi, R.B., Clarke, L.E., Burzomato, V., Kessaris, N., Anderson, P.N., Attwell, D., and Richardson, W.D. (2011). Dorsally and ventrally derived oligodendrocytes have similar electrical properties but myelinate preferred tracts. J. Neurosci. *31*, 6809–6819.

Van de Putte, T., Maruhashi, M., Francis, A., Nelles, L., Kondoh, H., Huylebroeck, D., and Higashi, Y. (2003). Mice lacking ZFHX1B, the gene that codes for Smad-interacting protein-1, reveal a role for multiple neural crest cell defects in the etiology of Hirschsprung disease-mental retardation syndrome. Am. J. Hum. Genet. *72*, 465–470.

Ventéo, S., Bourane, S., Méchaly, I., Sar, C., Abdel Samad, O., Puech, S., Blostein, R., Valmier, J., Pattyn, A., and Carroll, P. (2012). Regulation of the Na,K-ATPase gamma-subunit FXYD2 by Runx1 and Ret signaling in normal and injured non-peptidergic nociceptive sensory neurons. PLoS ONE *7*, e29852.

Weng, Q., Chen, Y., Wang, H., Xu, X., Yang, B., He, Q., Shou, W., Chen, Y., Higashi, Y., van den Berghe, V., et al. (2012). Dual-mode modulation of Smad signaling by Smad-interacting protein Sip1 is required for myelination in the central nervous system. Neuron *73*, 713–728.